


# Proximal Tubule Translational Profiling during Kidney Fibrosis Reveals Proinflammatory and Long Noncoding RNA Expression Patterns with Sexual Dimorphism

Haojia Wu,<sup>1,2</sup> Chun-Fu Lai,<sup>1,2,3</sup> Monica Chang-Panesso,<sup>1,2</sup> and Benjamin D. Humphreys<sup>1,2,4</sup> 

<sup>1</sup>Division of Nephrology, Departments of <sup>2</sup>Medicine and <sup>4</sup>Developmental Biology, Washington University in St. Louis School of Medicine, St. Louis, Missouri; and <sup>3</sup>Renal Division, Department of Internal Medicine, National Taiwan University Hospital, Taipei, Taiwan

## ABSTRACT

**Background** Proximal tubule injury can initiate CKD, with progression rates that are approximately 50% faster in males versus females. The precise transcriptional changes in this nephron segment during fibrosis and potential differences between sexes remain undefined.

**Methods** We generated mice with proximal tubule–specific expression of an L10a ribosomal subunit protein fused with enhanced green fluorescent protein. We performed unilateral ureteral obstruction surgery on four male and three female mice to induce inflammation and fibrosis, collected proximal tubule–specific and bulk cortex mRNA at day 5 or 10, and sequenced samples to a depth of 30 million reads. We applied computational methods to identify sex-biased and shared molecular responses to fibrotic injury, including up- and downregulated long noncoding RNAs (lncRNAs) and transcriptional regulators, and used *in situ* hybridization to validate critical genes and pathways.

**Results** We identified >17,000 genes in each proximal tubule group, including 145 G-protein–coupled receptors. More than 700 transcripts were differentially expressed in the proximal tubule of males versus females. The >4000 genes displaying altered expression during fibrosis were enriched for proinflammatory and profibrotic pathways. Our identification of nearly 150 differentially expressed proximal tubule lncRNAs during fibrosis suggests they may have unanticipated regulatory roles. Network analysis prioritized proinflammatory and profibrotic transcription factors such as *Irf1*, *Nfkb1*, and *Stat3* as drivers of fibrosis progression.

**Conclusions** This comprehensive transcriptomic map of the proximal tubule revealed sexually dimorphic gene expression that may reflect sex-related disparities in CKD, proinflammatory gene modules, and previously unappreciated proximal tubule–specific bidirectional lncRNA regulation.

JASN 31: 23–38, 2020. doi: <https://doi.org/10.1681/ASN.2019040337>

The medical and economic burden of CKD remains high worldwide and new therapies are needed.<sup>1,2</sup> The final common pathway of all progressive CKD is tubulointerstitial fibrosis, a process characterized histologically by myofibroblast expansion, extracellular matrix deposition, tubular atrophy, and peritubular capillary rarefaction. Activation of pericytes and mesenchymal stem cell–like stroma into proliferative, matrix-secreting myofibroblasts represent key steps in pathologic fibrosis.<sup>3</sup> Upstream stimuli for myofibroblast activation are

Received April 2, 2019. Accepted August 1, 2019.

H.W. and C.-F.L. contributed equally to this work.

Published online ahead of print. Publication date available at [www.jasn.org](http://www.jasn.org).

**Correspondence:** Dr. Benjamin D. Humphreys, Division of Nephrology, Department of Medicine, Washington University in Saint Louis School of Medicine, 660 South Euclid Avenue, Campus Box 8129, St Louis, MO 63110. Email: [humphreysbd@wustl.edu](mailto:humphreysbd@wustl.edu)

Copyright © 2020 by the American Society of Nephrology

less well understood but are of considerable interest because such pathways represent potential therapeutic targets. Increasing evidence implicates epithelial cells, in particular those of the proximal tubule (PT), as fibrosis-initiating cells. More expression quantitative trait loci for CKD are expressed in the PT than any other epithelial cell type.<sup>4</sup> Both ischemic and toxic insults to the kidney primarily affect the PT and these insults—whether genetic, ischemic, toxic, or otherwise—lead to adaptive and maladaptive cellular responses including cell cycle arrest, metabolic reprogramming, and secretion of profibrotic and proinflammatory factors leading to myofibroblast activation.<sup>5–7</sup> Both PT dysfunction and the secreted factors that are a consequence of the response to epithelial injury represent logical therapeutic targets to slow progression in CKD.

In part because they are unbiased, transcriptomic studies represent a powerful approach to better understand kidney disease. Bulk kidney transcriptional profiling has revealed core gene expression signatures in diabetic kidney disease, AKI and transition to chronic disease, unilateral ureteral obstruction (UUO), and new roles for B lymphocytes in dysfunctional kidney repair.<sup>8–11</sup> Cell-specific transcriptomic studies are increasingly favored over bulk approaches. Fluorescence-activated cell sorting can generate cell-specific transcriptome data, but is limited by the requirement for surface antibodies and the cellular dissociation and FACS procedure itself, which induces transcriptional stress responses.<sup>12</sup> Recently, single cell RNA-sequencing (scRNA-seq) approaches have been applied to understand mammalian kidney development and adult kidney in health and disease.<sup>13–16</sup> Although these are very powerful approaches, they still detect only the more highly expressed genes in a cell and may miss low to midlevel gene expression compared with cell-specific bulk RNA sequencing (RNA-seq).

The aim of our study was to generate a comprehensive and unbiased inventory of gene expression changes in the PT during fibrosis to serve as a scientific resource. We have previously validated translating ribosome affinity purification (TRAP) as a powerful means to generate cell-specific transcriptional profiles from podocytes and myofibroblasts in health and disease as well as the transcriptional response of all nephron epithelia to acute injury and repair.<sup>17–19</sup> We applied TRAP to the cortical PT in health, fibrosis, and between sexes, and compared it to whole cortex mRNAs. We report substantial differences in gene expression between male and female mice exist in healthy PT. We also define major proinflammatory gene modules upregulated in the PT after injury, implicating this cell type as a key driver of fibrosis. Finally, we report that over 143 long noncoding RNAs (lncRNAs) undergo both up- and downregulation in the PT, suggesting unappreciated cell-specific regulatory roles for lncRNAs in renal fibrosis.

## METHODS

### Animals

*Slc34a1-GFP-CreERT2* and *R26-EGFP-L10a* mouse lines were generated as described.<sup>19,20</sup> All animal care and experimental

### Significance Statement

Having a comprehensive transcriptional profile of the proximal tubule in health and fibrosis would likely enhance understanding of fibrosis and perhaps help explain why CKD progresses more quickly in males versus females. To obtain a more complete picture of gene expression in the proximal tubule, the authors performed deep translational profiling of this segment in a mouse model of kidney fibrosis. Their findings demonstrate substantial sex differences in transcripts expressed in proximal tubule cells of males versus females, and indicate that the proximal tubule drives fibrosis through inflammatory and profibrotic paracrine signaling. The study also identified 439 long noncoding RNAs expressed in the proximal tubule, 143 of which undergo differential regulation in fibrosis, suggesting that this type of RNA has unanticipated regulatory roles in kidney fibrosis.

protocols were conducted in accordance with the guidelines of the Institutional Animal Care and Use Committee of the Washington University in St. Louis (number 20180070). We crossed homozygous *Slc34a1-GFP-CreERT2* against homozygous *R26-EGFP-L10a* mice to generate compound heterozygous *Slc34a1-GFP-CreERT2*; *R26-EGFP-L10a* mice (hereafter referred to as *SLC34a1-eGFP-L10a*). Adult mice (8–12 weeks old) were used for all experiments. Tamoxifen (Sigma-Aldrich, St. Louis, MO) was dissolved in 3% (vol/vol) ethanol containing corn oil at a concentration of 10 mg/ml. To activate expression of *eGFP-L10a* in PT, mice received two doses of 3 mg of tamoxifen gavage over 3 days. This achieved >90% recombination in the cortical PTs.<sup>20</sup> Ten days after the last dose of tamoxifen, mice underwent left UUO surgery, as previously described.<sup>15</sup> Mice were euthanized and UUO and contralateral kidney (CLK) were harvested at 5 or 10 days after the surgery. Each group included three female and four male mice.

### TRAP and RNA-Seq

Purification of polysome-bound RNA from kidneys was performed according to our published reports<sup>18,19</sup> and the original publication.<sup>21</sup> RNA integrity was assessed using an RNA PicoChip (catalog number 5067–1513; Agilent Bioanalyzer). The Clontech SMARTer library kit (Takara Bio USA, Mountain View, CA) was used for cDNA library construction. Seven libraries were prepared in each group (three from female and four from male mice) and sequenced by HiSeq3000 to a depth of 30 million reads per sample. Reads were aligned to mm10 (Ensembl release 76) with STAR version 2.0.4b.<sup>22</sup> Gene counts were derived from the number of uniquely aligned unambiguous reads by Subread:featureCount version 1.4.5.<sup>23</sup> Transcript counts were produced by Sailfish version 0.6.3. Sequencing performance was assessed by measuring the total number of aligned reads; total number of uniquely aligned reads, genes, and transcripts detected; ribosomal fraction known junction saturation; and read distribution over known gene models with RSeQC version 2.3.<sup>24</sup> Bioinformatic analyses were carried out as described in Supplemental Methods.

### In Situ Hybridization

For each gene of interest, 400- to 800-bp DNA fragments were synthesized by PCR of cDNA with a 5' SP6 promoter and a 3' T7 promoter. Primer sequences are in Supplemental Methods. *In situ* hybridization (ISH) was performed in RNase-free conditions according to a published protocol<sup>9</sup> with modifications. Briefly, 15  $\mu$ m frozen tissue sections were fixed in 4% paraformaldehyde/PBS overnight at 4°C, permeabilized with Proteinase K (10  $\mu$ g/ml) for 20 minutes, postfixed, and incubated in acetylation solution (0.375% acetic anhydride) for 10 minutes. Slides were then incubated with digoxigenin-labeled sense or antisense riboprobes (0.5  $\mu$ g/ml riboprobes in hybridization buffer of 50% formamide, 50  $\mu$ g/ml yeast transfer RNA, 1% SDS, 50  $\mu$ g/ml heparin, and 5 $\times$  SSC) at 68°C overnight. Hybridization was followed by stringency washes, blocking (2% blocking reagent in PBS; Roche), and incubation with anti-digoxigenin-alkaline phosphatase antibody (catalog number 11093274910, 1:4000; Roche) overnight at 4°C. After washing, sections were treated with NTMT solution (100 mM sodium chloride, 100 mM Tris pH 9.5, 50 mM magnesium chloride, 0.1% Tween 20, 2 mM tetramisole) for 10 minutes. The final reaction was developed by adding chromogenic substrate (BM Purple, catalog number 11442074001; Roche) for 1–7 days until sufficient staining intensity was reached or signals started to appear in the negative control sections incubated by sense riboprobes. Sections were fixed by 4% paraformaldehyde/PBS again and then mounted by mounting medium (ProLong gold; ThermoFisher). Images were captured with a 20 $\times$  objective on a Zeiss Axio Scan Z1.

### Immunofluorescence Staining

After fixation in 4% paraformaldehyde/PBS for 90 minutes, kidney specimens were immersed in 30% sucrose/PBS overnight at 4°C, embedded in Tissue-Tek optimal cutting temperature compound (Miles Inc., Elkhart, IN) in liquid nitrogen, and stored at –80°C until cryostat sectioning.

Cryopreserved sections (6  $\mu$ m) were subsequently washed in PBS for 10 minutes, permeabilized by 0.25% Triton X-100/PBS for 10 minutes, and blocked with 5% BSA for 60 minutes at room temperature. Sections were incubated with chicken anti-GFP antibodies (catalog number GFP-1020, 1:300; Aves, Tigard, OR) at 4°C overnight. On the next day, the sections were washed twice in 0.1% Tween 20/PBS for 5 minutes each and then incubated with Alexa Fluor 488–conjugated donkey anti-chicken antibody (catalog number 703-545-155, 1:200; Jackson ImmunoResearch) and Cy3-conjugated anti-mouse- $\alpha$ SMA antibody (catalog number C6198, 1:400; Sigma-Aldrich) for 1 hour at room temperature. After three washes in 0.1% Tween 20/PBS for 5 minutes each, sections were colabeled with 4',6-diamidino-2-phenylindole (1:1000; Invitrogen) and mounted with ProLong Gold. The primary antibodies were omitted in sections as negative controls. Images were captured and processed using a confocal microscope (Eclipse Ti, Nikon). Sections were examined in a blinded fashion.

### Real-Time PCR

cDNA was synthesized by reverse transcription from extracted RNA by iScript cDNA Synthesis Kit (Bio-Rad Laboratories, Hercules, CA). Expression of target genes was determined by real-time quantitative PCR using the iTaq SYBR Green Supermix and the iQ5 Multicolor Real-Time PCR Detection System (Bio-Rad). Glyceraldehyde-3-phosphate dehydrogenase was used as the internal control.

### Data Availability

RNA-seq data for all samples have been deposited in the Gene Expression Omnibus (GSE125015). To increase rigor and reproducibility, the raw sequencing data as well as analysis files generated as part of this study were also uploaded into the (Re) Building a Kidney consortium database and are fully accessible at <https://doi.org/10.25548/16-E08W>.<sup>25</sup>

## RESULTS

### Translational Profiling of the PT during Fibrosis

We generated *Slc34a1-eGFPL10a* mice, performed UUO surgery, and euthanized mice at day 5 or 10 (Figure 1, A and B). eGFP-L10a expression was exclusively localized to the PT in a typical ribosomal nucleolar pattern (Figure 1C). At day 10 of UUO, *Acta2* ( $\alpha$ SMA) expression was dramatically induced in the interstitium as expected (Figure 1D). RNA quality from TRAP was excellent among all groups (average RNA integrity score of more than nine, Supplemental Figure 1A). We sequenced each sample to a depth of 30 million reads, enabling detection of >17,000 genes per sample (Supplemental Table 1 and Supplemental Figure 1A). This is more than twice the gene detection at less than half the sequencing depth compared with a recent report of bulk RNA-seq of microdissected PT which could detect approximately 7300 transcripts in the S1 and S2 segments (Supplemental Figure 1B and C).<sup>26</sup> There was a strong correlation between the biologic replicates in each group (Supplemental Figure 1D), suggesting high reproducibility across experiments.

Multidimensional scaling (MDS) analysis did not distinguish between sex or disease time points (day 5 UUO and day 10 UUO), whereas robust differences were detected between the sample types (PT or total cortex) and disease state (CLK and UUO; Figure 1E). As shown by the scatterplot of the whole transcriptome (Figure 1F) and quantitative PCR of selected genes (Figure 1G), PT samples were appropriately enriched for PT markers as expected (*Slc34a1*, *Slc5a2*, and *Slc2a2*) but not other kidney-type markers (e.g., *Nphs1* and *Synpo* for podocytes, *Aqp2* and *Aqp4* for collecting duct, *Col1a1* and *Acta2* for myofibroblasts, *Slc12a1* and *Umod* for loop of Henle, and *Pecam1* and *Emcn* for endothelial cells). Compared with total cortex, 119 transporters and ion channels were significantly enriched in the PT samples (false discovery rate [FDR] <0.05, Supplemental Table 2), consistent with the physiologic role of the PT in the kidney.

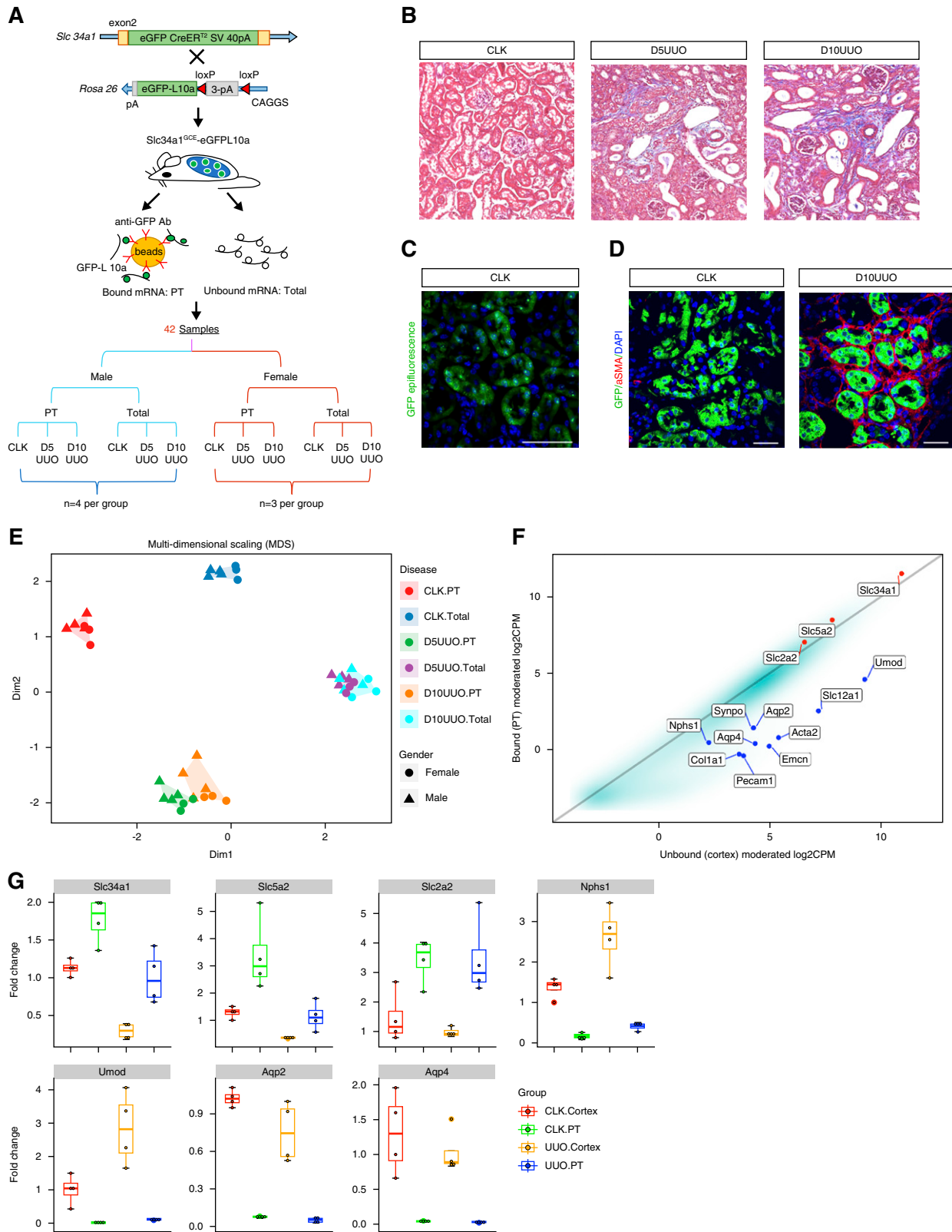


**Figure 1.** Successful translational profiling of PT using the *SLC34a1*-eGFP-L10a line. (A) Schematic illustrating the experimental workflow. (B) Trichrome stain showing collagen deposition in the kidney interstitium (male mice) after day 5 (D5UUO) and 10 (D10UUO) UUO. (C) Perinuclear and nucleolar expression of eGFP in PT (male mice), a pattern consistent with ribosomal location. Scale bar, 50  $\mu$ m. (D) Immunofluorescence staining shows a strong induction of interstitial  $\alpha$ SMA in the UUO kidney (male mice) and no

## TRAP Reveals Sexually Dimorphic Gene Expression in PT

MDS analysis on the PT samples showed no difference between day 5 and 10, so we combined those time points. The combined PT samples were separated based on both healthy versus disease and male versus female (Figure 2A). A total of 1013 genes were differentially expressed between male and female in healthy PT ( $FDR < 0.05$ ), and the number of differentially expressed genes (DEGs) was linearly correlated with the cutoff set for fold change ( $R^2 = 0.97$ ; Supplemental Figure 2A). When  $\log_2$  fold change was set to  $> 1$  and less than  $-1$  for up- and down-regulated genes, we detected 748 genes were differentially expressed between sexes (Supplemental Figure 2B). The vast majority of these sex-specific genes (approximately 95%) were located in autosomes rather than sex chromosomes (Figure 2B). In addition, 64.8% of these genes were also differentially expressed during UUO (Figure 2C, Supplemental Table 2). We validated two of these genes by ISH (male, *Cndp2*; female, *Hao2*) (Figure 2D) and additionally by reanalysis of published scRNA-seq data sets (female, *Kynu* and *Rdh16*; male, *Ces1f*, *Cyp4b1*, *Slc22a30*, and *Cyp2e1*; Figure 2E, Supplemental Table 3).<sup>15,16,27</sup> These expression differences may reflect some of the known sex-related disparities in CKD epidemiology<sup>28</sup> and progression.<sup>29</sup>

## PT Gene Signatures of Fibrosis

There were  $> 4000$  genes with altered PT expression after obstruction (Figure 3A). About 80% of the DEGs were shared between day 5 and 10 UUO versus CLK (Supplemental Figure 3A), suggesting most of the transcriptional changes occurring in this model of fibrosis happen by day 5, although we cannot exclude the contribution of changes in RNA stability. We observed a very similar trend when comparing day 5 versus day 10 whole cortex (Supplemental Figure 3B).

We validated expression of four upregulated genes (*Cstb*, *S100a10*, *Carhsp1*, and *RhoC*) in fibrotic PT by ISH (Figure 3B). None of these genes have known roles in the kidney. *Cstb* encodes cystatin B, a protease inhibitor of lysosomal cathepsins with antiapoptotic and anti-inflammatory actions in the brain and immune system.<sup>30</sup> *S100a10* encodes a plasminogen receptor that binds to plasminogen and facilitates its activation to plasmin, a protease that regulates matrix remodeling. Intriguingly, *S100a10* has been shown to promote mesenchymal transition of epithelial cells in cancer models.<sup>31</sup> *Carhsp1* encodes calcium-regulated heat stable protein 1 containing a cold-shock domain and two RNA-binding motifs.<sup>32</sup> It binds to the 3' untranslated region of TNF- $\alpha$  mRNA, doubling transcript

$t_{1/2}$  and increasing TNF- $\alpha$  proinflammatory signaling.<sup>33</sup> Finally, *RhoC* encodes Ras homolog family member C, a small GTPase that regulates cell motility, cell division, and protein trafficking. Although *RhoC* has never been described in the kidney, Rho-kinase inhibitors are known to be antifibrotic.<sup>34</sup> We observed strong downregulation of genes expressed in differentiated epithelia. *Slc22a8*, also known as organic anion transporter 3, is strongly expressed in cortical PT, but after UUO it was almost undetectable (Figure 3B).

We next quantified the added specificity that PT TRAP provides compared with profiling of whole cortex. We compared the DEGs identified in the PT to those identified in the whole cortex. Of the DEGs from fibrotic PT, 22.7% were not differentially expressed in whole cortex (Figure 3C, Supplemental Figure 3C). By contrast, 26.3% of the DEGs from whole cortex did not change in PT (Figure 3D, Supplemental Figure 3C). Thus PT-specific profiling by TRAP is both more sensitive and more specific than bulk cortex profiling, despite the fact that PT makes up the majority of cortical cell mass.

We then compared the disease genes identified in this study to the disease signature identified in our prior TRAP data using a *Six2-eGFPL10a* line. Although this comparison was limited because these two data sets were generated from different Cre driver lines (*Slc34a1-CreER<sup>2</sup>* versus *Six2-Cre*), different animal models (UUO versus ischemia reperfusion injury [IRI]), and different profiling platforms (RNA-seq versus microarray); we found 64.9% of disease DEGs identified in the *Six2* data set (IRI versus sham) were detected by this study (UUO versus control) (Supplemental Figure 4A). We then performed gene ontology (GO) analysis separately on the upregulated DEGs unique to *Six2* TRAP, unique to *Slc34a1* TRAP, and shared by both (Supplemental Figure 4B). Interestingly, the top enriched terms for the *Six2* DEGs, *Slc34a1* DEGs, and shared DEGs were apoptosis, inflammation, and fibrosis, respectively (Supplemental Figure 4C). These results are consistent with the tubular disease phenotypes we expect for IRI and UUO.

## PT Gene Signatures for Epithelial-to-Mesenchymal Transition, Fatty Acid Metabolism, Hedgehog Signaling, and G protein-coupled receptors

Our comprehensive data set can be used to assess the role of the PT in fibrogenesis. Tubular epithelia were once thought to directly contribute to the interstitial myofibroblast pool in fibrosis through a process of “full epithelial-to-mesenchymal transition” (full EMT). Lineage tracing data have disproven that hypothesis, although epithelia do take on a mesenchymal phenotype within the tubule.<sup>35,36</sup> We selected candidate

expression in eGFP-positive proximal tubular cells. (E) Sample clustering in MDS plot. Scale bar, 50  $\mu$ m. (F) Robust enrichment of PT-specific genes through scatterplot of normalized expression values in bound RNA (PT) versus unbound RNA (whole cortex). (G) Validation of cell type specificity of the *SLC34a1-eGFPL10a* line using quantitative PCR. PT markers, *Slc34a1*, *Slc5a2* (*Sglt2*) and *Slc2a2* (*Glut2*); podocyte markers, *Nphs1* and *Synpo*; loop of Henle markers, *Slc12a1* and *Umod*; collecting duct markers, *Aqp2* and *Aqp4*; endothelial markers, *Emcn* and *Pecam1*; myofibroblast markers, *Col1a1* and *Acta2*. Statistical analysis was performed using one-way ANOVA to compare data among groups (four male mice per group). Ab, antibody; CPM, count per million; DAPI, 4',6-diamidino-2-phenylindole.



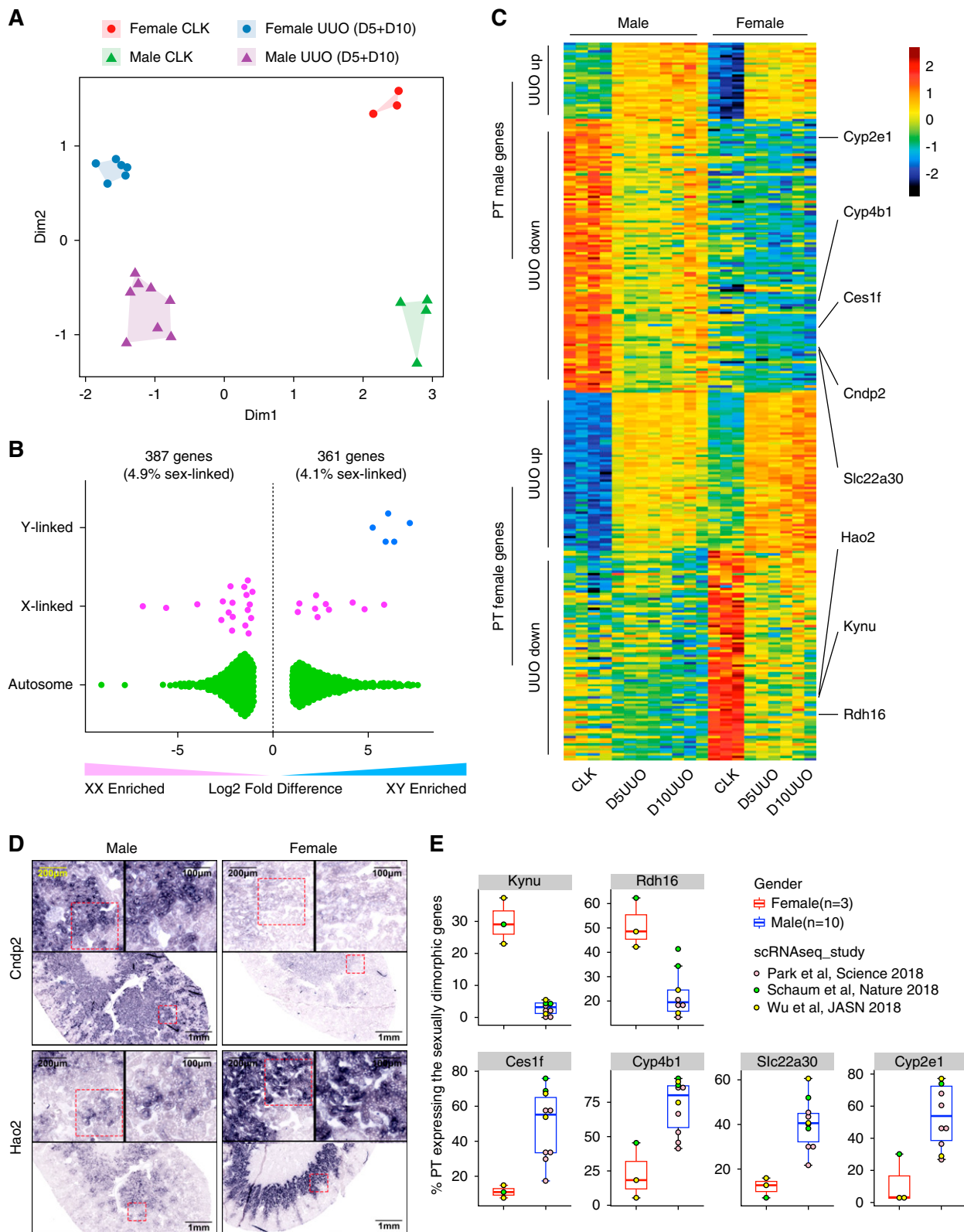


**Figure 2.** TRAP reveals sexually dimorphic gene expression in PT. (A) MDS plot shows separation of the PT TRAP samples by disease and sex. (B) Chromosomal distribution of sexually dimorphic genes (FDR<0.05, log fold change >1 or less than -1). (C) Heatmap visualizing the sex-specific genes that are differentially expressed in UUO kidney. (D) Sex-specific expression pattern of *Cndp2* and *Hao2* validated by RNA ISH. Red boxes indicate region enlarged. (E) Reanalysis of published scRNA-seq data sets confirms the specific expression of *Kynu* and *Rdh16* in female PT, and *Ces1f*, *Cyp4b1*, *Slc22a30*, and *Cyp2e1* in male PT. Statistical analysis was performed using the Welch *t* test to compare data between sexes. D5, day 5; D10, day 10.

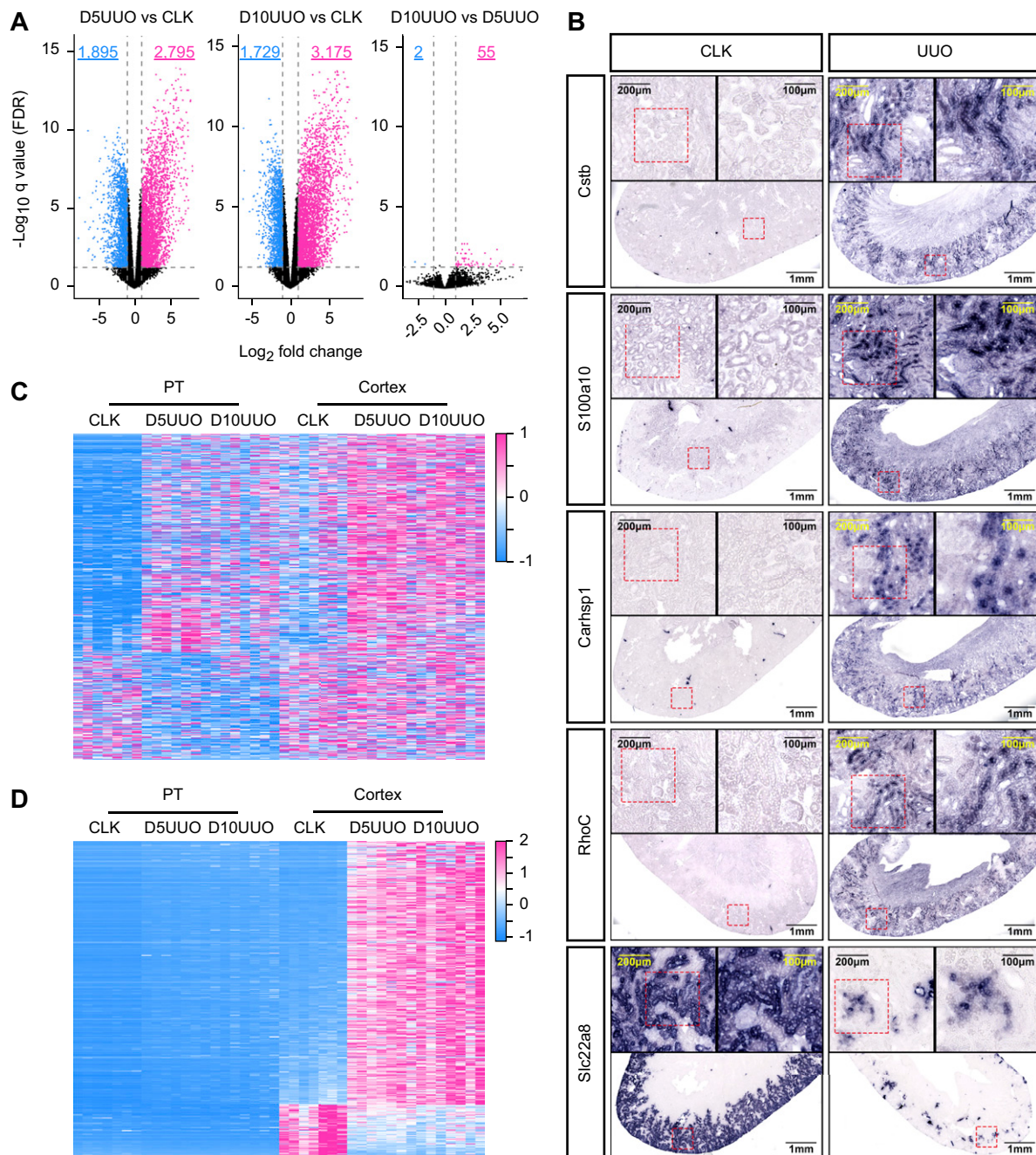


**Figure 3.** Validation of PT-specific injury signature in fibrosis. (A) Volcano plots revealing widespread gene expression changes in PT beginning at UUO day 5 (D5UUO). Longer kidney obstruction time (day 10 [D10UUO]) altered the PT transcriptome only minimally. (B) RNA ISH of select PT injury responsive genes identified from TRAP analysis. Representative images were obtained from female kidneys. Red boxes indicate region enlarged. (C) Heatmap illustrating genes whose expression are altered in fibrotic PT but not detected in whole cortex. (D) Heatmap of expression profiles in all samples for DEGs that are changed during UUO in whole cortex but not in the PT. FDR<0.05, log fold change >1 or less than -1.

EMT markers, including *Snai1*, *Snai2*, *Twist*, and various matrix metalloproteases and collagens and visualized their expression in PT versus whole cortex. UUO significantly altered the expression of these EMT markers in both PT and whole cortex (Supplemental Table 2), but the expression level of these genes in the UUO kidney was much lower in PT than

in whole cortex (Figure 4A, Supplemental Figure 5A), suggesting a trivial contribution of tubular EMT to kidney fibrosis. Concordant with this result, reanalysis our UUO scRNA-seq data revealed that fewer than 3% of PT cells expressed the EMT markers (*Acta2*, *Col1a1*, *Col3a1*, *Fnl1*, and *Mmp2*) in the UUO kidney compared with the healthy control

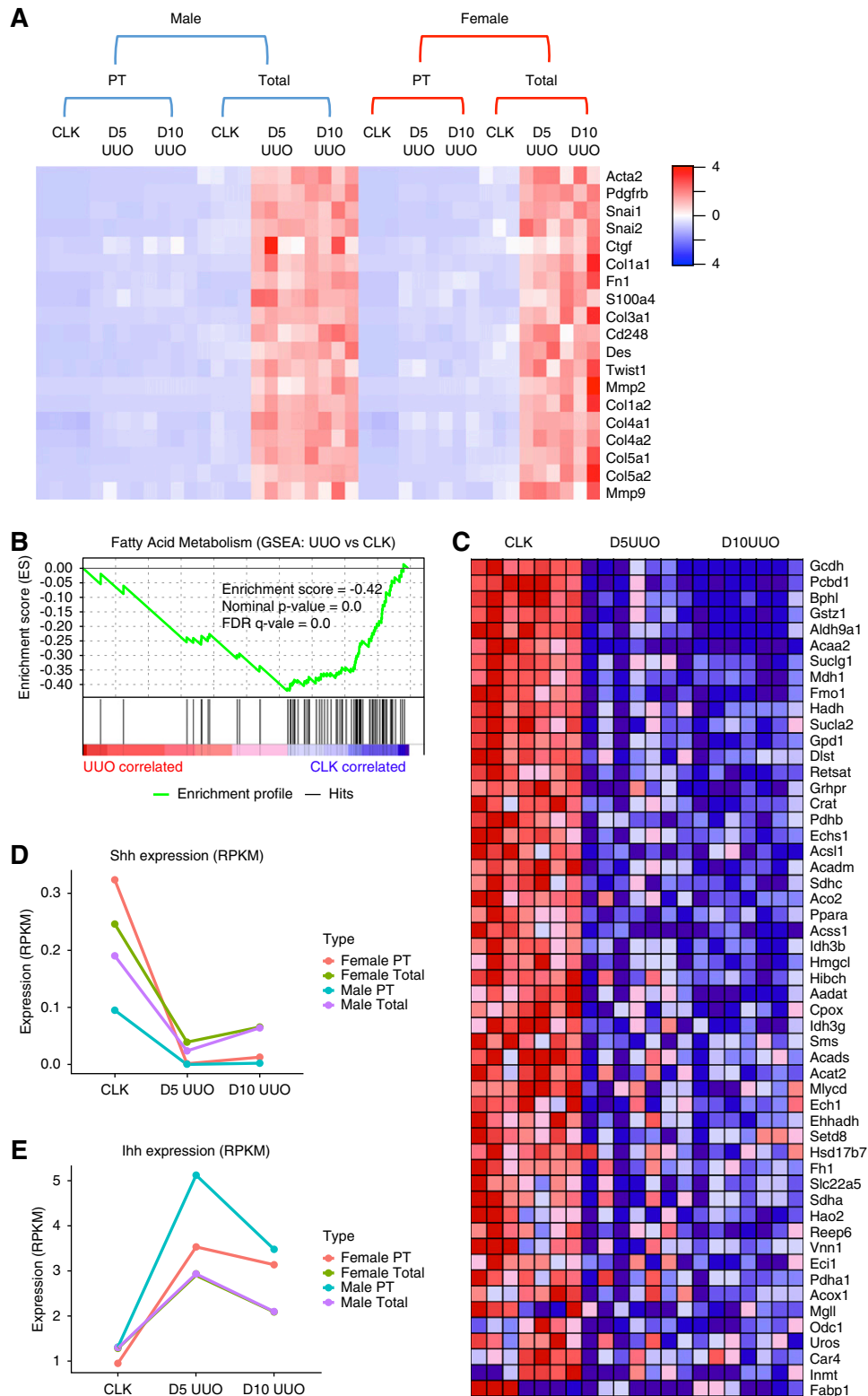


**Figure 4.** Evaluation of epithelial-to-mesenchymal transition, fatty acid metabolism, and hedgehog ligand gene expression signatures. (A) Heatmap showing the expression of EMT markers in whole kidney but not PT. (B) Gene set enrichment analysis (GSEA) confirms defective fatty acid metabolism in PT during UUO. The total height of the curve indicates the extent of enrichment, with the normalized enrichment score (ES), *P* value, and FDR value indicated. (C) Heatmap of leading edge genes in the fatty acid metabolism gene set. (D) Expression of *Ihh* in PT by reads per kilobase of transcript per million mapped reads (RPKM) value. (E) Expression of *Shh* in PT by RPKM value. D5UUO, 5 days after UUO; D10UUO, 10 days after UUO.



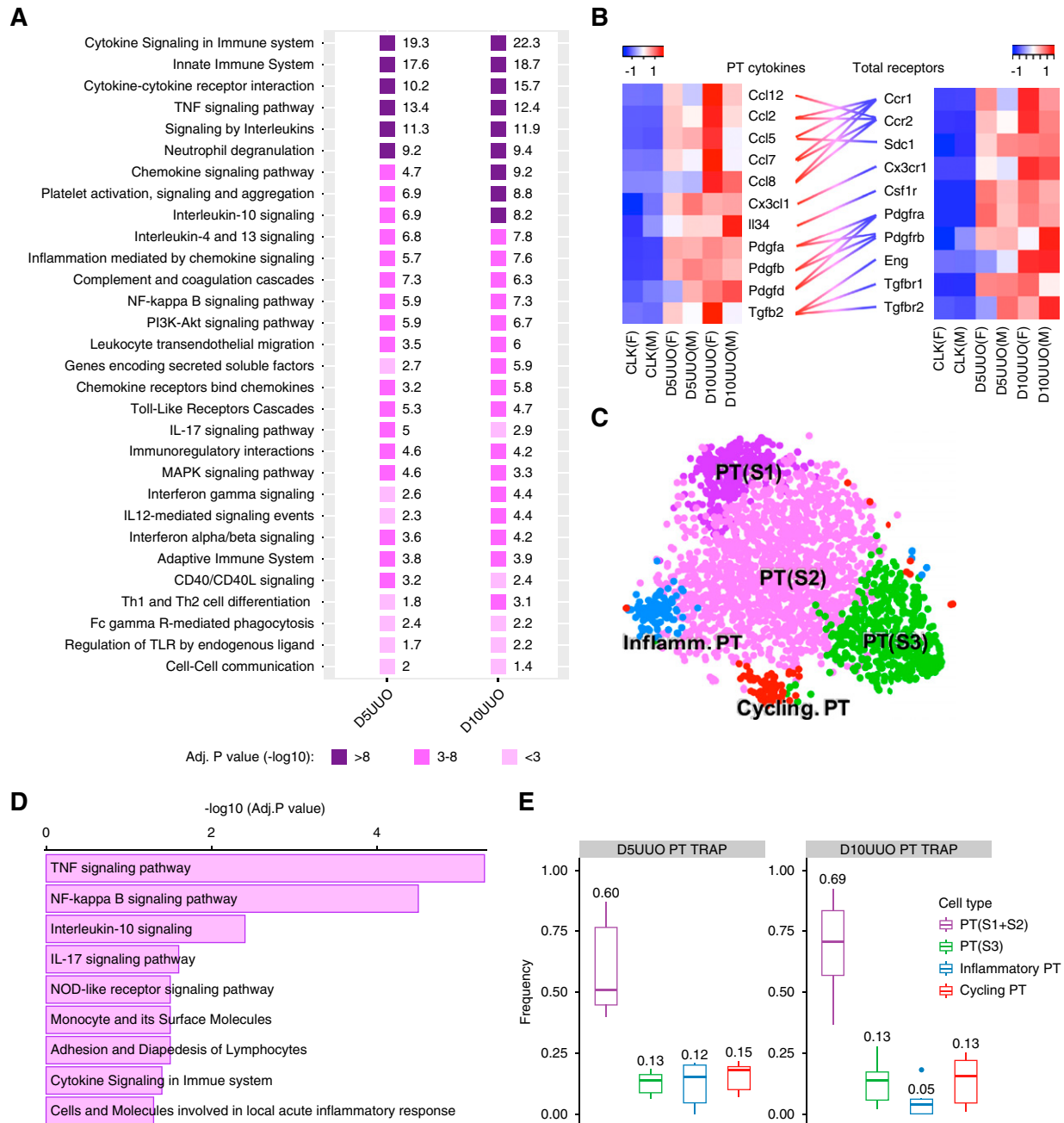


**Figure 5.** A strong proinflammatory gene expression signature is detected in PT during kidney fibrosis. (A) Pathway analysis using the DEG lists from PT (day 5 UUO [D5UUO] versus CLK and day 10 UUO [D10UUO] versus CLK). (B) Ligand-receptor analysis illustrating the interaction between PT and other cell types in the cortex. Heatmap showing the expression of cytokines/growth factors in PT (left) and their cognate receptors in the whole cortex (right). Straight lines connect the ligand-receptor pairs. (C) Reclustering of proximal tubular cells from day 14 UUO scRNA-seq data set identifies five PT subtypes including a subcluster expressing inflammatory markers. (D) Pathway analysis using the marker gene list from the inflammatory PT cluster. (E) Deconvolution of the subtype composition in the PT TRAP samples using the molecular signature identified from scRNA-seq. Adj., adjusted; F, female; inflamm., inflammatory; M, male; Th1/2, T helper cell 1/2; TLR, Toll-like receptor.

(Supplemental Figure 5B), and no mesenchymal transition state was identified in the PT subtypes of the day 14 UUO kidney.

We then tested if our TRAP data supported defective fatty acid metabolism in PT during UUO, because this has recently been shown to contribute to fibrosis progression.<sup>5,37</sup> Gene set

enrichment analysis using DEGs revealed the majority of fatty acid metabolism-related genes were enriched in the CLK group (Figure 4B), with 83.3% of the genes in this GO term (60 of 72) significantly downregulated in the tubular fraction of the UUO kidney (Figure 4C).

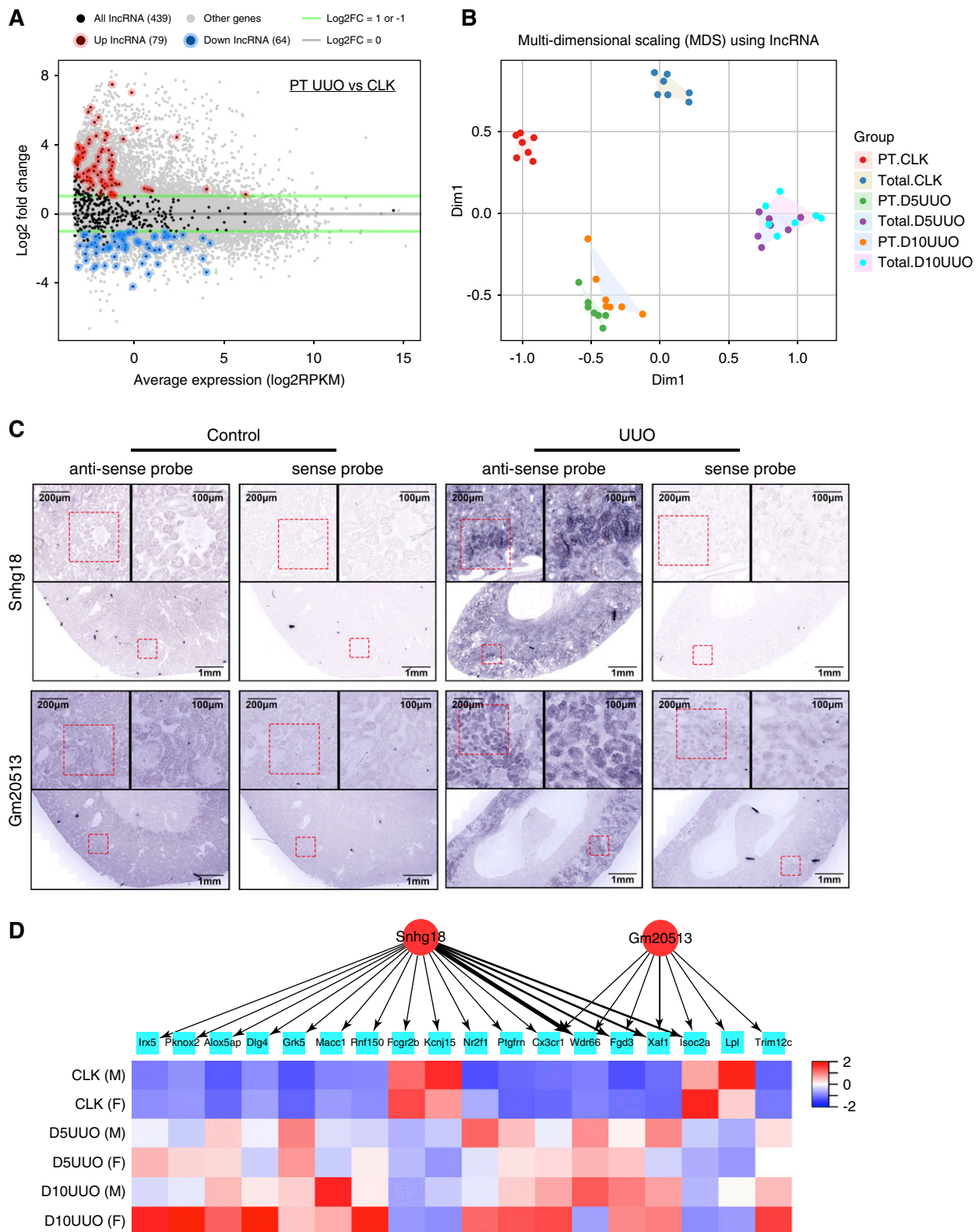


**Figure 6.** Many lncRNAs are detected and undergo differential regulation in PT during fibrosis. (A) MA plot displaying the differentially expressed lncRNAs in PT (UUO versus CLK). (B) MDS plot for the PT TRAP samples according to lncRNA expression profiles alone. (C) ISH validates two PT lncRNAs selected from the DEG list (UUO versus CLK). Data were obtained from male kidneys. Red boxes indicate region enlarged. (D) Network approach to show the protein coding mRNAs that might be targeted by *Snhg18* and *Gm20513*. Nodes are lncRNAs (circle) and their target mRNAs (square). Edge sizes are determined by the energy (absolute log scale) required for

There is controversy within the literature regarding whether PT upregulates Indian hedgehog (*Ihh*)<sup>38</sup> or sonic hedgehog (*Shh*) after injury. We clearly identified upregulation of PT *Ihh*,<sup>38</sup> whereas *Shh* was expressed at almost undetectable levels at baseline and subsequently underwent downregulation after UUO, despite reports to the contrary (Figure 4, D and E).<sup>39,40</sup>

G protein-coupled receptors (GPCRs) constitute the largest family for approved drugs, with a third of the 364 human endo-GPCRs serving as targets for approved drugs.<sup>41</sup> We examined GPCR expression in PT and identified 132 GPCRs expressed at baseline. Of these GPCRs, 91 underwent up- or downregulation during fibrosis, and 13 additional GPCRs were expressed *de novo* during fibrosis (Supplemental Table 2). Of these 13 *de novo* upregulated GPCRs, four of them send proinflammatory signals in response to their ligands, including the formyl peptide receptor *Fpr2*, the chemokine receptor *Cxcr3*, the free fatty acid receptor *Ffar2*, and the sphingosine-1-phosphate receptor *S1pr4*. Intriguingly, *Ffar2* also regulates energy metabolism as does another of these upregulated receptors, the chemokine-like receptor 1 *Cmklr1*, suggesting possible mechanisms underlying the metabolic switch in PT during fibrosis (Figure 4C).

#### PT Acquires a Proinflammatory Phenotype during Fibrosis

Previous studies implicate immune cell infiltration in the progression of kidney fibrosis in the mouse UUO model.<sup>42–44</sup> Consistent with these studies, analysis of the total cortex samples detected a variety of markers for various immune cell types (B cells, CD4<sup>+</sup> T cells, CD8<sup>+</sup> T cells, CD14<sup>+</sup> monocytes, dendritic cells, CD16<sup>+</sup> monocytes, megakaryocytes, and natural killer cells) that were all upregulated during UUO (Supplemental Figure 6C). We hypothesize proximal tubular cells play an important role in recruiting the immune cells to the fibrotic kidney by secretion of cytokines and chemokines. To test this hypothesis, we performed pathway enrichment analysis on the upregulated DEGs identified from UUO versus CLK using the ToppFun Suite. This highlighted differential regulation of two key pathways in PT during fibrosis: immune response and inflammation (Figure 5A). Receptor-ligand analysis revealed very robust proinflammatory (*Ccl2*, -5, -7, -8, -12, *IL34*) and profibrotic (*Pdgfa*, *Pdgfb*, *Pdgfd*, *Tgfb*) ligand upregulation in PT (Figure 5B), with their cognate receptors expressed in whole kidney, implicating PT as a central driver of the inflammatory and fibrotic cascade.

Integrative analysis of our previously published scRNA-seq of PT in UUO<sup>15</sup> confirmed the strong induction of *Il34* and *Pdgfd* during kidney fibrosis (Supplemental Figure 6A). Furthermore, a separate cluster in the day 14 UUO data set was classified as a PT subtype that acquired a proinflammatory

transitional state based on the expression of unique signatures identified from unsupervised clustering analysis (Figure 5C). Very similar pathways were identified in this proinflammatory PT cluster (Figure 5D) compared with the pathways we have observed to be enriched in the UUO TRAP (Figure 5A). To validate the existence of these PT subtypes in our TRAP samples, we applied the BSEQ-sc algorithm to estimate cell heterogeneity within each TRAP group from the UUO kidneys, based on the PT-subtype signature identified from scRNA-seq analysis of the day 14 UUO kidney. This revealed a consistent fraction of these subpopulations in the PT from scRNA-seq and TRAP (Figure 5E, Supplemental Figure 6B).

#### Identification of Differentially Expressed lncRNAs during Fibrosis

lncRNAs are a very large (up to 30,000 different lncRNAs in humans) and diverse class of transcribed RNAs of longer than 200 nucleotides. They do not encode known proteins, and regulate gene expression through diverse mechanisms. lncRNA expression is regulated developmentally, in a tissue- and cell-specific fashion as well as in disease. In a bulk kidney transcriptomic survey, Arvaniti *et al.*<sup>45</sup> found that UUO altered the expression of 126 lncRNA genes, 77 of which were intergenic lncRNAs. We could reproduce 63.6% of these intergenic lncRNAs when we compared the mRNA expression in whole cortex between UUO and control using the same significance threshold (FDR<0.05). But we also identified an additional 183 differentially expressed lncRNAs not identified by Arvaniti and colleagues (Supplemental Figure 7A). Because recent studies have reported that lncRNAs can be pulled down by TRAP,<sup>46,47</sup> we examined lncRNA expression in PT. A total of 439 lncRNAs were identified in our PT data set (Figure 6A). Differential gene analysis revealed 79 upregulated and 64 downregulated lncRNAs in PT during UUO compared with control (Figure 6A). Strikingly, MDS analysis using the lncRNAs grouped the samples in the same way as when using the whole transcriptomes (Figures 1E and 6B), suggesting the ribosome-bound lncRNAs are expressed in a highly cell-specific fashion both in health and fibrosis.

RNA ISH analysis of *Snhg18* (average reads per kilobase of transcript per million mapped reads, 87.1) and *Gm20513* (average reads per kilobase of transcript per million mapped reads, 1.0), two representative lncRNAs with high expression and low expression, respectively, confirmed the expected UUO-induced expression patterns (Figure 6C, Supplemental Figure 7B). Because a major role of ribosome-bound lncRNA is regulation of mRNA translation,<sup>48</sup> we next determined the potential target mRNAs that were regulated by *Snhg18* and *Gm20513*. Using a computation prediction tool (<http://rtools.cbrc.jp/LncRRISearch/>), we were able to rank the target

lncRNA-mRNA interaction (LncRRI tools). Heatmap showing the target genes that are differentially expressed in PT during UUO. D5UUO, 5 days after UUO; D10UUO, 10 days after UUO; F, female; log<sub>2</sub>FC, log<sub>2</sub> fold change; M, male; RPKM; reads per kilobase of transcript per million mapped reads.

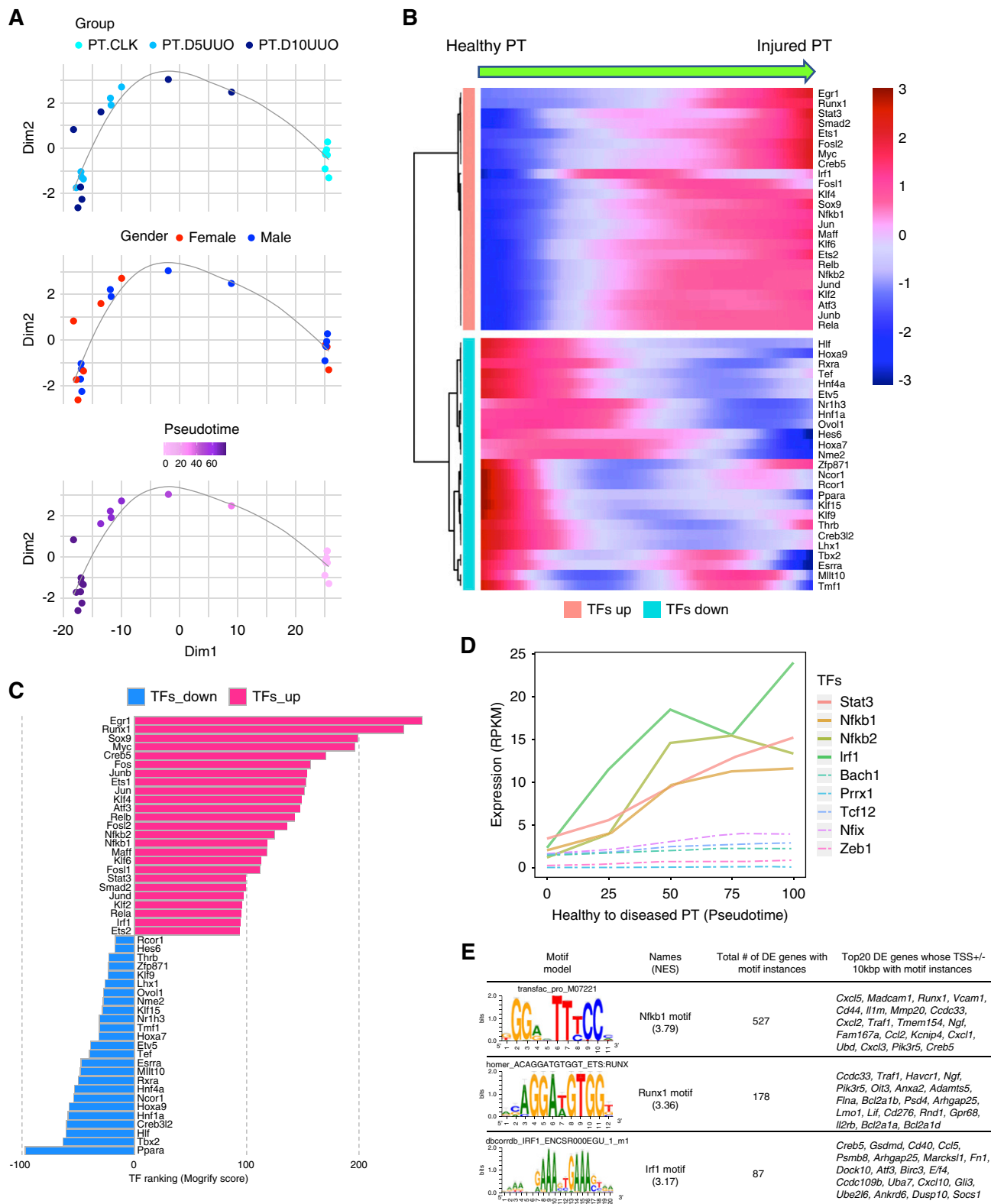


**Figure 7.** Identification of transcription factors and regulatory regions driving disease progression in kidney fibrosis. (A) Sample state ordering in reduced dimension space using the Monocle algorithm. Samples are color coded by actual time point, sex, and pseudotime. (B) Top differentially expressed transcription factors along the pseudotime from healthy to fibrotic PT. (C) Transcription factor (TF) ranking using the influence score as determined by the Mogrify algorithm. Negative score indicates downregulated transcription factors. (D) Visualization of the reads per kilobase of transcript per million mapped reads (RPKM) values for the selected transcription factors.



mRNAs that interacted with *Snhg18* and *Gm20513* based on their known expression in PT, although it should be emphasized that these tools can be inaccurate and should be viewed as a means to generate hypotheses. The expression of some of these target genes were also altered by UUO (Figure 6D), suggesting but not proving the possibility that translation of these genes might be regulated by lncRNA during fibrosis. Detailed annotations for putative target genes for *Snhg18* and *Gm20513* revealed that some of these genes were related to proinflammatory responses such as *Fcgr2b*, *Cx3cr1*, *Lpl*, and *Alox5ap* (Supplemental Table 4). *Lpl* was also involved in fatty acid metabolism; *Fcgr2b* and *Lpl* were also members of the profibrotic GO terms including extracellular region and extracellular space (Supplemental Table 4).

### Data-Driven Analysis Identifies Key Transcription Factors that Drive Disease Progression in Kidney Fibrosis

We next sought to identify the key drivers controlling disease progression in kidney fibrosis. We implemented a data-driven approach, Monocle,<sup>49</sup> to order the TRAP samples in pseudotime based on global gene expression changes rather than time point. In this analysis, samples were not ordered according to time point or sex, revealing heterogeneity between samples from the same time points (Figure 7A). We could validate the pseudotemporal ordering of the global gene expression by examining expression of known fibrosis regulators on the pseudotime trajectory (*Stat3*<sup>50</sup> and *Nfkb1*;<sup>51</sup> Supplemental Figure 8, A and B). We then performed a differential gene test across pseudotime and highlighted the top transcription factors derived from the DEG list (Figure 7B). We then used a regulatory network approach, the Mogrify algorithm (<http://www.mogrify.net>),<sup>52,53</sup> to rank these transcription factors according to importance. This implicated a number of previously unrecognized transcription factors such as *Maff*, *Klf6*, and *Creb5* as well as a variety of transcription factors known to play roles in kidney injury, such as *Stat3*,<sup>50</sup> *Nfkb2*,<sup>51</sup> *Irf1*,<sup>54</sup> *Egr1*,<sup>55</sup> and *Jund*<sup>56</sup> (Figure 7C). Notably, the top transcriptional regulators control inflammation (e.g., *Stat3*, *Nfkb1*, *Nfkb2*, and *Irf1*), whereas transcription factors that regulate EMT did not increase in expression (*Bach1*, *Prrx1*, *Tcf12*, *Nfix*, and *Zeb1*) as predicted by the Mogrify algorithm (Figure 7D). In addition, we identified 150 NF- $\kappa$ B target genes that were markedly upregulated in PT after UUO (Supplemental Table 2).

Finally, we performed motif enrichment analysis in the  $\pm 10$ -kbp region surrounding the transcription start site of the DEGs (see Methods) to identify candidate transcription factors that might be driving differential expression. The three binding motifs significantly enriched in 527, 178,

and 87 DEGs, respectively, were for *Nfkb1*, *Runx1*, and *Irf1* (Figure 7E, Supplemental Table 5). These three motifs were also identified by the Mogrify algorithm, providing independent confirmation for their potential importance in regulating fibrosis.

## DISCUSSION

In this study, we tested the hypothesis that TRAP could provide enhanced sensitivity and specificity for PT gene expression detection to better define the role of this cell type in renal fibrosis. The results demonstrate that TRAP outperforms bulk as well as microdissection approaches. Whole-cortex profiling will miss about a quarter of the DEGs in PT, while also identifying another quarter of genes that are differentially expressed but are not expressed in PT. Thus TRAP improves both sensitivity and specificity, even for the most abundant kidney cell type. Although laser capture microdissection or tubule segment microdissection certainly improves specificity, when we compared our data set to those generated by such approaches, TRAP identified at least twice as many total genes at half the sequencing depth.

Although scRNA-seq is a powerful and increasingly adopted transcriptomic technology in kidney studies, bulk cell-specific approaches like TRAP offer complementary advantages in certain applications. Our PT molecular map identified about 17,000 genes expressed in PT, whereas scRNA-seq has more limited gene detection sensitivity. Regulatory genes may be expressed at lower levels, so sensitive gene detection may be required to measure those transcripts. Our ability to define 145 GPCRs illustrates this point. Overall these results suggest TRAP can be a good option when (1) an appropriate Cre driver line is available to activate eGFP-L10a expression in the desired cell types; (2) cell-specific but not single-cell transcriptomics is desired; (3) the transcriptome is of more interest than the transcriptome; and (4) a simple, relatively inexpensive method that does not require any specialized equipment is optimal.

This molecular map of PT in fibrosis also provided important biologic insights concerning kidney fibrosis. A finding of central importance from our study is that the PT actively drives fibrosis through activation of proinflammatory and profibrotic pathways. This is consistent with a model whereby nephron epithelia are the first cells to sense and react to damage, whether from albuminuria, genetic, toxic, or immune causes. These findings are consistent with Beckerman *et al.*<sup>57</sup> whose transcriptome analysis of microdissected tubulointerstitium also

factors that are related to inflammation (solid lines) and EMT (dashed lines). (E) Motif analysis on the list of upregulated genes identified in PT after UUO. Three representative motifs that are significantly enriched within 10 kbp upstream and downstream of the transcription start site (TSS) for the DEGs are shown. D5UUO, 5 days after UUO; D10UUO, 10 days after UUO; DE, differentially expressed; NES, normalized enrichment score.

identified strong proinflammatory gene modules that correlated with estimated glomerular filtration loss.

Several large observational studies have shown differing rates of progression in CKD between men and women, but the molecular explanation for this epidemiologic observation remains unknown. Recently, using data from the Chronic Renal Insufficiency Cohort Study, Ricardo and colleagues reported that women in this cohort had both a lower risk of CKD progression, ESKD, and death, compared with men.<sup>29</sup> Although there may be many potential reasons for this disparity, our finding that a substantial number of genes exhibit sexually dimorphic expression both at baseline and during fibrosis suggests gene expression differences may be at least partly responsible. The McMahon group (A. Ransick, N. O. Lindström, J. Liu, Z. Qin, J.-J. Guo, G. F. Alvarado, *et al.*, unpublished observations) has recently also reported that the PT, among all nephron segments, displays a large degree of sexually dimorphic gene expression, confirming our results.

Finally, a recent estimate suggested >98% of transcribed RNAs are not translated to protein in eukaryotic cells and most of these noncoding transcripts are classified as lncRNA.<sup>58</sup> It is increasingly clear that lncRNA may participate in the pathogenesis of many kidney diseases, through the mechanisms of chromatin modification, transcriptional regulation, post-transcriptional control, or by functioning as decoy or molecular sponges.<sup>59–61</sup> Many lncRNAs have recently been reported to contain functional small open reading frames that may be translated into peptides.<sup>47,62,63</sup> We identified many lncRNAs differentially expressed during renal fibrosis by TRAP sequencing (Figure 6, A–E, Supplemental Table 2), presumably indicating that these lncRNAs are bound by mRNA undergoing translation consistent with other recent analyses.<sup>46,47</sup> It should be noted that functional lncRNAs may not require a poly-A tail, and whether we isolated such lncRNAs is not clear from our analysis.

In conclusion, this article provides an unbiased and deep description of PT gene expression in health, during fibrosis and across sexes. Our study highlights the power of the TRAP approach to provide high-quality, cell-specific mRNA and reinforces the concept that the PT is a critical, active driver of cortical fibrosis through regulation of proinflammatory and profibrotic pathways.

## ACKNOWLEDGMENTS

Dr. Chang-Panesso designed and carried out experiments and analyzed results. Dr. Humphreys designed experiments, analyzed results, and wrote the manuscript. Dr. Lai and Dr. Wu designed and carried out experiments, analyzed results, and contributed to writing of the manuscript.

## DISCLOSURES

Dr. Humphreys reports personal fees from Merck, personal fees from Janssen, personal fees from Medimmune, personal fees from Roche, personal

fees from Celgene, personal fees from Chinook Therapeutics, personal fees from Genetech, grants from Biogen Idec, grants from Janssen, and other from Chinook Therapeutics, outside the submitted work.

## FUNDING

This work was supported by National Institutes of Health, National Institute of Diabetes and Digestive and Kidney Diseases grants DK103740 and DK107374 (to Dr. Humphreys).

## SUPPLEMENTAL MATERIAL

This article contains the following supplemental material online at <http://jasn.asnjournals.org/lookup/suppl/doi:10.1681/ASN.2019040337/-/DCSupplemental>.

Supplemental Figure 1. TRAP sample quality control.

Supplemental Figure 2. Sexually dimorphic genes in proximal tubule.

Supplemental Figure 3. Disease signature for kidney fibrosis.

Supplemental Figure 4. Comparison of the DEG identified from this study and the published *Six2*-TRAP dataset.

Supplemental Figure 5. EMT marker expression in TRAP-seq and scRNA-seq.

Supplemental Figure 6. Proximal tubule pro-inflammatory gene expression and subtype composition revealed by scRNA-seq.

Supplemental Figure 7. lincRNA expression in UUO kidneys.

Supplemental Figure 8. Sample ordering validation by transcription factors known to be upregulated in proximal tubule during kidney fibrosis.

Supplemental Table 1. Sequencing characteristics.

Supplemental Table 2. TRAP gene expression summary.

Supplemental Table 3. PT sexually dimorphic gene expression from scRNA-seq dataset.

Supplemental Table 4. Annotations of putative target genes for lncRNAs *Snhg18* and *Gm20513*.

Supplemental Table 5. Enriched PT binding motifs during fibrosis.

Supplemental Methods.

## REFERENCES

1. Glasscock RJ, Warnock DG, Delanaye P: The global burden of chronic kidney disease: Estimates, variability and pitfalls. *Nat Rev Nephrol* 13: 104–114, 2017
2. United States Renal Data System: 2017 USRDS annual data report: Epidemiology of kidney disease in the United States, Bethesda, MD, National Institutes of Health, National Institute of Diabetes and Digestive and Kidney Diseases, 2017
3. Humphreys BD: Mechanisms of renal fibrosis. *Annu Rev Physiol* 80: 309–326, 2018
4. Wu H, Uchimura K, Donnelly EL, Kirita Y, Morris SA, Humphreys BD: Comparative analysis and refinement of human PSC-derived kidney organoid differentiation with single-cell transcriptomics. *Cell Stem Cell* 23: 869–881.e868, 2018
5. Kang HM, Ahn SH, Choi P, Ko YA, Han SH, Chinga F, *et al.*: Defective fatty acid oxidation in renal tubular epithelial cells has a key role in kidney fibrosis development. *Nat Med* 21: 37–46, 2015

6. Zhou HL, Zhang R, Anand P, Stomberski CT, Qian Z, Hausladen A, et al.: Metabolic reprogramming by the S-nitroso-CoA reductase system protects against kidney injury. *Nature* 565: 96–100, 2019
7. Canaud G, Brooks CR, Kishi S, Taguchi K, Nishimura K, Magassa S, et al.: Cyclin G1 and TASC regulate kidney epithelial cell G<sub>2</sub>-M arrest and fibrotic maladaptive repair. *Sci Transl Med* 11: eaav4754, 2019
8. Woroniecka KI, Park AS, Mohtat D, Thomas DB, Pullman JM, Susztak K: Transcriptome analysis of human diabetic kidney disease. *Diabetes* 60: 2354–2369, 2011
9. Liu J, Kumar S, Dolzhenko E, Alvarado GF, Guo J, Lu C, et al.: Molecular characterization of the transition from acute to chronic kidney injury following ischemia/reperfusion. *JCI Insight* 2: 94716, 2017
10. Cippà PE, Sun B, Liu J, Chen L, Naesens M, McMahon AP: Transcriptional trajectories of human kidney injury progression. *JCI Insight* 3: 123151, 2018
11. Cippà PE, Liu J, Sun B, Kumar S, Naesens M, McMahon AP: A late B lymphocyte action in dysfunctional tissue repair following kidney injury and transplantation. *Nat Commun* 10: 1157, 2019
12. Adam M, Potter AS, Potter SS: Psychrophilic proteases dramatically reduce single-cell RNA-seq artifacts: A molecular atlas of kidney development. *Development* 144: 3625–3632, 2017
13. Lindström NO, Guo J, Kim AD, Tran T, Guo Q, De Sena Brandine G, et al.: Conserved and divergent features of mesenchymal progenitor cell types within the cortical nephrogenic niche of the human and mouse kidney. *J Am Soc Nephrol* 29: 806–824, 2018
14. Menon R, Otto EA, Kokoruda A, Zhou J, Zhang Z, Yoon E, et al.: Single-cell analysis of progenitor cell dynamics and lineage specification in the human fetal kidney. *Development* 145: dev164038, 2018
15. Wu H, Kiritia Y, Donnelly EL, Humphreys BD: Advantages of single-nucleus over single-cell RNA sequencing of adult kidney: Rare cell types and novel cell states revealed in fibrosis. *J Am Soc Nephrol* 30: 23–32, 2019
16. Park J, Shrestha R, Qiu C, Kondo A, Huang S, Werth M, et al.: Single-cell transcriptomics of the mouse kidney reveals potential cellular targets of kidney disease. *Science* 360: 758–763, 2018
17. Grgic I, Hofmeister AF, Genovese G, Bernhardt AJ, Sun H, Maarouf OH, et al.: Discovery of new glomerular disease-relevant genes by translational profiling of podocytes in vivo. *Kidney Int* 86: 1116–1129, 2014
18. Grgic I, Krautzberger AM, Hofmeister A, Lalli M, DiRocco DP, Fleig SV, et al.: Translational profiles of medullary myofibroblasts during kidney fibrosis. *J Am Soc Nephrol* 25: 1979–1990, 2014
19. Liu J, Krautzberger AM, Sui SH, Hofmann OM, Chen Y, Baetscher M, et al.: Cell-specific translational profiling in acute kidney injury [published correction appears in *J Clin Invest* 124: 2288, 2014]. *J Clin Invest* 124: 1242–1254, 2014
20. Kusaba T, Lalli M, Kramann R, Kobayashi A, Humphreys BD: Differentiated kidney epithelial cells repair injured proximal tubule. *Proc Natl Acad Sci U S A* 111: 1527–1532, 2014
21. Heiman M, Schaefer A, Gong S, Peterson JD, Day M, Ramsey KE, et al.: A translational profiling approach for the molecular characterization of CNS cell types. *Cell* 135: 738–748, 2008
22. Dobin A, Davis CA, Schlesinger F, Drenkow J, Zaleski C, Jha S, et al.: STAR: Ultrafast universal RNA-seq aligner. *Bioinformatics* 29: 15–21, 2013
23. Liao Y, Smyth GK, Shi W: FeatureCounts: An efficient general purpose program for assigning sequence reads to genomic features. *Bioinformatics* 30: 923–930, 2014
24. Wang L, Wang S, Li W: RSeQC: Quality control of RNA-seq experiments. *Bioinformatics* 28: 2184–2185, 2012
25. Humphreys BD: (Re)Building a Kidney Consortium, <https://doi.org/10.25548/16-E08W>. 2019
26. Lee JW, Chou CL, Knepper MA: Deep sequencing in microdissected renal tubules identifies nephron segment-specific transcriptomes. *J Am Soc Nephrol* 26: 2669–2677, 2015
27. Tabula Muris Consortium: Single-cell transcriptomics of 20 mouse organs creates a Tabula Muris. *Nature* 562: 367–372, 2018
28. Carrero JJ, Hecking M, Chesnaye NC, Jager KJ: Sex and gender disparities in the epidemiology and outcomes of chronic kidney disease. *Nat Rev Nephrol* 14: 151–164, 2018
29. Ricardo AC, Yang W, Sha D, Appel LJ, Chen J, Krousel-Wood M, et al.: CRIC Investigators: Sex-related disparities in CKD progression. *J Am Soc Nephrol* 30: 137–146, 2019
30. Kopitar-Jerala N: The role of stefin B in neuro-inflammation. *Front Cell Neurosci* 9: 458, 2015
31. Bydoun M, Sterea A, Weaver ICG, Bharadwaj AD, Waisman DM: A novel mechanism of plasminogen activation in epithelial and mesenchymal cells. *Sci Rep* 8: 14091, 2018
32. Nastasi T, Scaturro M, Bellafiore M, Raimondi L, Beccari S, Cestelli A, et al.: PIPPin is a brain-specific protein that contains a cold-shock domain and binds specifically to H1 degrees and H3.3 mRNAs. *J Biol Chem* 274: 24087–24093, 1999
33. Pfeiffer JR, McAvoy BL, Fecteau RE, Deleault KM, Brooks SA: CARHSP1 is required for effective tumor necrosis factor alpha mRNA stabilization and localizes to processing bodies and exosomes. *Mol Cell Biol* 31: 277–286, 2011
34. Nagatoya K, Moriyama T, Kawada N, Takeji M, Oseto S, Murozono T, et al.: Y-27632 prevents tubulointerstitial fibrosis in mouse kidneys with unilateral ureteral obstruction. *Kidney Int* 61: 1684–1695, 2002
35. Humphreys BD, Lin SL, Kobayashi A, Hudson TE, Nowlin BT, Bonventre JV, et al.: Fate tracing reveals the pericyte and not epithelial origin of myofibroblasts in kidney fibrosis. *Am J Pathol* 176: 85–97, 2010
36. Kramann R, DiRocco DP, Humphreys BD: Understanding the origin, activation and regulation of matrix-producing myofibroblasts for treatment of fibrotic disease. *J Pathol* 231: 273–289, 2013
37. Chung KW, Lee EK, Lee MK, Oh GT, Yu BP, Chung HY: Impairment of PPAR $\alpha$  and the fatty acid oxidation pathway aggravates renal fibrosis during aging. *J Am Soc Nephrol* 29: 1223–1237, 2018
38. Fabian SL, Penchev RR, St-Jacques B, Rao AN, Sipilä P, West KA, et al.: Hedgehog-Gli pathway activation during kidney fibrosis. *Am J Pathol* 180: 1441–1453, 2012
39. Zhou D, Li Y, Zhou L, Tan RJ, Xiao L, Liang M, et al.: Sonic hedgehog is a novel tubule-derived growth factor for interstitial fibroblasts after kidney injury. *J Am Soc Nephrol* 25: 2187–2200, 2014
40. Ding H, Zhou D, Hao S, Zhou L, He W, Nie J, et al.: Sonic hedgehog signaling mediates epithelial-mesenchymal communication and promotes renal fibrosis. *J Am Soc Nephrol* 23: 801–813, 2012
41. Sriram K, Insel PA: G protein-coupled receptors as targets for approved drugs: How many targets and how many drugs? *Mol Pharmacol* 93: 251–258, 2018
42. Vielhauer V, Allam R, Lindenmeyer MT, Cohen CD, Draganovici D, Mandelbaum J, et al.: Efficient renal recruitment of macrophages and T cells in mice lacking the duffy antigen/receptor for chemokines. *Am J Pathol* 175: 119–131, 2009
43. Tapmeier TT, Fearn A, Brown K, Chowdhury P, Sacks SH, Sheerin NS, et al.: Pivotal role of CD4<sup>+</sup> T cells in renal fibrosis following ureteric obstruction. *Kidney Int* 78: 351–362, 2010
44. Han H, Zhu J, Wang Y, Zhu Z, Chen Y, Lu L, et al.: Renal recruitment of B lymphocytes exacerbates tubulointerstitial fibrosis by promoting monocyte mobilization and infiltration after unilateral ureteral obstruction. *J Pathol* 241: 80–90, 2017
45. Arvaniti E, Moulos P, Vakrakou A, Chatziantoniou C, Chadjiachristos C, Kavvadas P, et al.: Whole-transcriptome analysis of UUO mouse model of renal fibrosis reveals new molecular players in kidney diseases. *Sci Rep* 6: 26235, 2016
46. Zhou P, Zhang Y, Ma Q, Gu F, Day DS, He A, et al.: Interrogating translational efficiency and lineage-specific transcriptomes using ribosome affinity purification. *Proc Natl Acad Sci U S A* 110: 15395–15400, 2013
47. Bazin J, Baerenfaller K, Gosai SJ, Gregory BD, Crespi M, Bailey-Serres J: Global analysis of ribosome-associated noncoding RNAs unveils new

- modes of translational regulation. *Proc Natl Acad Sci U S A* 114: E10018–E10027, 2017
48. Pircher A, Gebetsberger J, Polacek N: Ribosome-associated ncRNAs: An emerging class of translation regulators. *RNA Biol* 11: 1335–1339, 2014
  49. Qiu X, Mao Q, Tang Y, Wang L, Chawla R, Pliner HA, et al.: Reversed graph embedding resolves complex single-cell trajectories. *Nat Methods* 14: 979–982, 2017
  50. Bienaimé F, Muorah M, Yammine L, Burtin M, Nguyen C, Baron W, et al.: Stat3 controls tubulointerstitial communication during CKD. *J Am Soc Nephrol* 27: 3690–3705, 2016
  51. Sanz AB, Sanchez-Niño MD, Ramos AM, Moreno JA, Santamaria B, Ruiz-Ortega M, et al.: NF-kappaB in renal inflammation. *J Am Soc Nephrol* 21: 1254–1262, 2010
  52. Rackham OJ, Firas J, Fang H, Oates ME, Holmes ML, Knaupp AS, et al.: FANTOM Consortium: A predictive computational framework for direct reprogramming between human cell types. *Nat Genet* 48: 331–335, 2016
  53. Zhu Q, Fisher SA, Dueck H, Middleton S, Khaladkar M, Kim J: PIVOT: Platform for interactive analysis and visualization of transcriptomics data. *BMC Bioinformatics* 19: 6, 2018
  54. Wang Y, John R, Chen J, Richardson JA, Shelton JM, Bennett M, et al.: IRF-1 promotes inflammation early after ischemic acute kidney injury. *J Am Soc Nephrol* 20: 1544–1555, 2009
  55. Ho LC, Sung JM, Shen YT, Jheng HF, Chen SH, Tsai PJ, et al.: Egr-1 deficiency protects from renal inflammation and fibrosis. *J Mol Med (Berl)* 94: 933–942, 2016
  56. Pillebout E, Weitzman JB, Burtin M, Martino C, Federici P, Yaniv M, et al.: JunD protects against chronic kidney disease by regulating paracrine mitogens. *J Clin Invest* 112: 843–852, 2003
  57. Beckerman P, Qiu C, Park J, Ledo N, Ko YA, Park AD, et al.: Human kidney tubule-specific gene expression based dissection of chronic kidney disease traits. *EBioMedicine* 24: 267–276, 2017
  58. Mattick JS: The central role of RNA in human development and cognition. *FEBS Lett* 585: 1600–1616, 2011
  59. Zhou Q, Huang XR, Yu J, Yu X, Lan HY: Long noncoding RNA arid2-IR is a novel therapeutic target for renal inflammation. *Mol Ther* 23: 1034–1043, 2015
  60. Lorenzen JM, Thum T: Long noncoding RNAs in kidney and cardiovascular diseases. *Nat Rev Nephrol* 12: 360–373, 2016
  61. Lai CF, Chen YT, Gu J, Nerbonne JM, Lin CH, Yang KC: Circulating long noncoding RNA DKFZP434I0714 predicts adverse cardiovascular outcomes in patients with end-stage renal disease. *Int J Cardiol* 277: 212–219, 2019
  62. Chekulaeva M, Rajewsky N: Roles of long noncoding RNAs and circular RNAs in translation. *Cold Spring Harb Perspect Biol* 11: a032680, 2018
  63. Li LJ, Leng RX, Fan YG, Pan HF, Ye DQ: Translation of noncoding RNAs: Focus on lncRNAs, pri-miRNAs, and circRNAs. *Exp Cell Res* 361: 1–8, 2017